Anthropogenic influences alter the response and seasonality of evapotranspiration: A case study over two High Mountain Asia basins

Fadji Z. Maina[1,2*], Sujay V. Kumar[1]

[1] NASA Goddard Space Flight Center, Hydrological Sciences Laboratory, Greenbelt, Maryland, USA
[2] University of Maryland, Baltimore County, Goddard Earth Sciences Technology and Research Studies and Investigations, Baltimore, Maryland, USA

*Corresponding Author: fadjizaouna.maina@nasa.gov

Key points:

1. Climate and human induced greening have different effects on evapotranspiration and therefore the land-atmosphere interactions.
2. Though irrigation-induced greening rises pre-monsoon evapotranspiration, the latter decreases in post-monsoon due to groundwater depletion.
3. Climate-induced greening increases evapotranspiration because the energy demand is easily met.

Abstract

Earth's vegetation has been increasing over the past decades, altering water and energy cycles by changing evapotranspiration (ET). Greening, caused by climatic and anthropogenic factors, has high rates in High Mountain Asia (HMA). Here we focus on two HMA basins (the Yangtze and the Ganges-Brahmaputra) to contrast the impacts of climate- and human- induced greening on ET. Though the rate of greening is similar in both basins, anthropogenic influences lead to dissimilar responses in ET. In the Yangtze, climate-induced greening increases ET, with the increase in moisture being high enough to meet the ET demand. In the Ganges-Brahmaputra, irrigation-induced greening does not alter annual ET, only pre-monsoon ET increases. The dry season declines in water storage due to pumping decrease ET, while laboriously meeting the demand. This study provides a representative example of the contrasting influences of climate induced and anthropogenic driven processes on the seasonality of ET.

Keywords: High Mountain Asia, Greening, Evapotranspiration, irrigation, warming, climate change

Plain Language Summary

The significant increases in vegetation occurring on Earth are susceptible to altering the climate by affecting evapotranspiration. However, the responses in evapotranspiration to the changes in vegetation depend on the drivers of greening. Here we use High Mountain Asia as a testbed to contrast the impacts of greening on evapotranspiration. Irrigation-induced greening leads to an increase in transpiration and evapotranspiration in the pre-monsoon. However, because irrigation decreases water storage it decreases evapotranspiration in the post-monsoon. Climate-induced greening, on the contrary, increases both evapotranspiration and water storage.

1. Introduction

Terrestrial Evapotranspiration (ET) is a key component of the global energy and water cycles (Jung et al., 2010) and the second largest water vapor flux at continental scales. Around 60% of the global annual precipitation returns to the atmosphere through ET (Findell et al., 2011; Oki & Kanae, 2006). ET connects the land surface with the atmosphere and is composed of: (1) transpiration (T), the dominant process of ET (Jasechko et al., 2013), (2) evaporation (E), and (3) canopy evaporation of intercepted rainfall (I). The coupling of water and energy cycles is generally dominated by T and E with I being the smaller contributor to overall ET. Assessing the long-term variability in ET and its drivers is essential for disentangling the impacts of climate change and human activities on the interactions between the land and the atmosphere (Douville et al., 2013).

Anthropogenic activities and CO_2 fertilization induce greening on Earth (Piao et al., 2020; Zhu et al., 2016), which affects the atmosphere and the climate by changing ET (Piao et al., 2020; Zeng, Peng, et al., 2018; Zeng, Piao, et al., 2018). Greening impacts the climate by cooling the land surface temperature (Kiehl & Trenberth, 1997; Shen et al., 2015) and influencing the redistribution of heat and moisture and the ratio of T to ET (T/ET; Forzieri et al., 2020; Yang et al., 2022). Consequently, greening impacts the surface energy partitioning, which exerts control on the atmospheric boundary layer and regulates the land-atmosphere feedback (Forzieri et al., 2020; Puma et al., 2013; Williams & Torn, 2015).

Human activities and global warming have intensified ET (Douville et al., 2013; Hu & Mo, 2022; Zeng et al., 2012, 2014, 2016; Zeng, Peng, et al., 2018; K. Zhang et al., 2015) and more than 50% of this ET intensification over the past 30 years is attributed to greening (Zhang et al., 2015). Increases in ET can slow down global warming as ET contributes to 70% of cooling on Earth (Cook et al., 2011; Shen et al., 2015; Zeng et al., 2017). However, because greening is caused by

many drivers, the responses in ET to greening are diverse, yet little is known about the responses in ET to the different drivers of greening (Hu & Mo, 2022; Z. Niu et al., 2019; Yang et al., 2022; Zeng, Piao, et al., 2018).

High Mountain Asia (HMA), home to the largest reservoir of freshwater outside the polar region, experiences one of the highest rates of greening on Earth (Chen et al., 2019; Cortés et al., 2021; Liu et al., 2021; Maina et al., 2022; Piao et al., 2015a, 2015b). HMA covers nine countries, including China, Bangladesh, and India, and encompasses hydrologic basins such as the Yangtze, and Ganges-Brahmaputra. HMA's greening is caused by anthropogenic activities (irrigation) and a changing climate, i.e., increases in precipitation and decreases in snow cover (Maina et al., 2022). Because of the diversity of the drivers of HMA's greening and its high increases, the region is a good candidate for studying the impacts of greening on ET.

Here, we contrast the impacts of irrigation- and climate- induced greening on ET as well as its components T and E over two key basins of HMA, to demonstrate how anthropogenic influences alter the hydrologic response and seasonality. This is enabled through the development of a multivariate analysis, consisting of five variables that capture the effects of human activities (irrigation and groundwater depletion) and a changing climate into the land surface model Noah-multi-parameterization (Noah-MP; Niu et al., 2011). The multivariate observational constraints in this analysis enable an improved representation of the hydrological processes from the lower atmosphere to the bedrock.

In the Ganges-Brahmaputra, irrigation triggers the highest increases in leaf area index (LAI) in addition to depleting groundwater (Maina et al., 2022). The Yangtze, covered by forests, experiences greening because of increasing precipitation and warming. Over HMA, warming is occurring at a rate that is double the global average. This increases soil moisture by decreasing the

snow cover and creates an environment favorable to vegetation growth by making the growing season longer. Though previous studies have linked increases in ET to vegetation growth over HMA, these studies did not contrast the diverse responses in ET to the different types of greening (Yang et al., 2022; Piao, et al., 2018; Zhang et al., 2015). Therefore, here we focus on the following science objectives: 1) Contrast the relative impacts of climate- and human management-driven processes on the ET variations; 2) Quantify how the seasonality of these external drivers impacts ET patterns and Water Use Efficiency (WUE); and 3) Assess how anthropogenic water abstractions impact the regional responses in meeting the ET demand. The study, thus, provides a representative example of quantifying the heterogeneous changes in ET in response to climate variability and anthropogenic influences, which is important for many water resource applications (Sherwood & Fu, 2014; Syed et al., 2014; Webster et al., 2010).

2. Study area and Methods

2.1.The Ganges-Brahmaputra and the Yangtze basins

The Ganges-Brahmaputra and the Yangtze (Figure 1) are two of the most important hydrologic basins of HMA (Viviroli et al., 2007), home to over a billion people. The Ganges-Brahmaputra with a draining area of approximately 2 million km^2, is a transboundary basin that encompasses the Ganges River, which has its source in the glaciated area of Gomukh in the Himalayas, and the Brahmaputra River which also originates from the Himalayas in the glaciated zone of Lake Mana Sarovar. This basin stretching out from the Himalayas to the Bay of Bengal has one of the highest irrigated areas in the world due to intense agriculture (Figure 1b). Croplands represent the dominant land cover of the Ganges-Brahmaputra, evergreen and mixed forests are mainly found in the Himalayas (Figure 1a). The Yangtze spans from the Tibetan Plateau to the

East China Sea. In this work, however, we only study the Upper Yangtze, located above Three Gorges Dam.

2.2.Land Surface Modeling

We utilize the Noah-MP (Niu et al., 2011) version 4.0.1, a widely used model that simulates key land-atmosphere interactions in addition to groundwater changes (Niu et al., 2011). The surface energy balance is computed at the canopy layer and the ground surface. The soil with a depth of 2 m is divided into four layers, and the water movement is simulated using the Richards equation (Richards, 1931). An unconfined aquifer is added below the 2 m of the soil column.

For the HMA simulations, we use (1) an ensemble precipitation generated by Maina et al., (2022) by applying a localized probability-matched method (Clark, 2017) to blend three gridded precipitation products (the Integrated Multi-satellitE Retrievals for Global Precipitation Measurement IMERG (Huffman et al., 2015), the Climate Hazards group Infrared Precipitation with Stations CHIRPS (Funk et al., 2015), and the ECMWF Reanalysis ERA5 (Hersbach et al., 2020)) and (2) meteorological forcing (temperature, shortwave, and longwave radiation, wind speed, relative humidity, etc.) generated by downscaling ERA5 following Xue et al., (2019), and (2022). The model uses the MERIT-DEM (Multi Error Removed Improved Terrain Digital Elevation Model; (Yamazaki et al., 2017)) elevation, slope, and aspect. The landcover is based on the Moderate Resolution Imaging Spectroradiometer (MODIS; (Friedl, Mark & Sulla-Menashe, Damien, 2019)) at a resolution of 500 m, and the soil types are derived from the International Soil Reference and Information Centre (ISRIC, 2020) at a 250 m resolution. The model has a resolution of 5 km and was initialized by running it twice from 1990 to 2018. We, then, perform the assimilation from 2003 to 2020, a time frame based on the availability of the remotely sensed data. We assimilated five different remote-sensing data products:

- (1) European Space Agency Climate Change Initiative (ESA CCI) Soil Moisture: we assimilated the combined datasets using the one-dimensional ensemble Kalman Filter (EnKF) algorithm (EnKF; Reichle et al., 2002). In this approach, the observations are rescaled to the model climatology using the cumulative density function (CDF) approach, following Kumar et al., (2012, 2014).
- (2) MODIS LAI: We assimilated the MCD15A2H Version 6 of MODIS (Myneni et al., 2015) using the EnKF approach following Kumar et al., (2019). The updated LAI from assimilation is used to update the leaf biomass by dividing the LAI value with the specific leaf area, which varies with vegetation type (Liu et al., 2016).
- (3) a Snow Water Equivalent (SWE) reconstruction: We assimilated the Kraaijenbrink et al., (2021)'s dataset, which employs a temperature index melt model (Hock, 2003) using the EnKF approach as described by Kumar et al., (2019).
- (4) GRACE GSFC mascons terrestrial water storage (TWS) were assimilated using the one-dimensional ensemble Kalman smoother (EnKS) as described in Kumar et al., (2016) and Zaitchik et al., (2008).
- (5) Irrigation: spatiotemporal values of the applied irrigated water were generated by combining a static irrigation dataset, the Global Irrigated Area Map (GIAM), and a time-varying irrigation map for India from Ambika et al., (2016). We directly added this estimated applied irrigated water as a source in the model using the sprinkler irrigation scheme for simplification though other irrigation schemes are used in the region. Also, the impacts of tillage are not accounted for. The applied irrigated water is subtracted from groundwater following (Nie et al., 2018).

A model ensemble of size 20 was created by perturbing the hourly meteorological forcing inputs (precipitation, downward longwave, and shortwave radiation), the modeled and the observed variables i.e., soil moisture, LAI, SWE, snow depth, and groundwater storage. The selected perturbation parameters are shown in Supplementary Table 1.

Note that we also performed an open loop simulation i.e., a simulation without any assimilation accounting for the changes in climate only. The improved utility of the multivariate data assimilation has been validated by comparing the simulated streamflow, runoff, groundwater storage, ET, and snow cover to those obtained from other reanalyses, remotely sensed, and groundwater measurements (Maina & Kumar, 2023, Maina et al., 2023). Here, we discuss the comparisons between the trends in simulated ET (Figure 2 and Supplementary Figure 3) and gross primary production (GPP, Supplementary Figure 1) and those derived from remotely sensed data.

3. Results and discussions

3.1.Greening and its influence on ET

In HMA, the highest increases in LAI (>0.005 m^2/m^2/year) occur in the Ganges-Brahmaputra and the Yangtze (Figure 2a). In the Ganges-Brahmaputra, greening mainly occurs over the croplands and the forests, however, the relative changes in LAI over the croplands remain higher than in the forests. Because of their lack of vegetation and high elevations, greening is not observed over the Himalayas. In the eastern part of the basin (i.e., the Brahmaputra), greening is very low (<0.001 m^2/m^2/year) because of the absence of irrigation and the climatological decrease in precipitation (Supplementary Figure 1). Though the Yangtze is predominantly covered by mixed forests and croplands (which are not irrigated), LAI increases only in mid- to low- elevation areas due to increasing precipitation (Maina et al., 2022), at a rate similar to the rates observed in the Ganges-Brahmaputra.

The Himalayas and the Brahmaputra have a decrease in ET (>7.5 mm/year) due to a decrease in water availability and the absence of greening, while the areas subject to greening in the Ganges-Brahmaputra have a mix of positive and no significant trends in ET (up to 15mm/year, Figure 2b). The highest increases in ET are in the Chambal and Betwa basins, which are not subject to irrigation, and areas near the Bay of Bengal. The Yangtze has a low to a statistically increasing trend in ET (>10 mm/year). Although greening is occurring at similar rates in both basins, the responses in ET to greening are different. As shown in Supplementary Figures 2 and 3 comparing the trends in ET obtained with the open loop and the multivariate assimilation, such an increasing trend in ET (which consistent with observations) is only observed while accounting for greening and groundwater depletion, while the open loop has statistically non-significant trends in ET in both the Ganges-Brahmaputra and the Yangtze basins.

Figure 2g depicts the comparisons of the trends in the simulated and remotely sensed ET from MOD16 (Running, Steve et al., 2017) and the Global Land Evaporation Amsterdam Model (GLEAM; (Martens et al., 2017)). The trends in simulated ET agree with the trends in ET derived from MOD16 and GLEAM. 86% of GLEAM and 79% of MOD16 trends were captured by the model. In the Yangtze, the increases in ET agree with the trends in remotely sensed products. In the Ganges-Brahmaputra, the zero and positive trends in ET over the croplands agree with those of MOD16 and GLEAM. However, while our model indicates a decreasing trend in ET in the Himalayas, both MOD16 and GLEAM indicate a positive trend in ET. Such differences are likely arising from the assimilation of GRACE TWS, which has a decreasing trend in this region. The assimilation of GRACE data reduces subsurface moisture storage, which leads to a reduction in ET (Girotto et al., 2017).

3.2.Impacts of greening on E, T, WUE, and the ratio ET/PET

In the Ganges-Brahmaputra, the trends in E are mostly a mix of decreasing and statistically insignificant (~4 mm/year, Figure 2c) patterns. Only the Chambal and the Betwa basins have sparse areas with increasing trends in E (up to 10 mm/year). On the other hand, T is increasing in all areas that experience greening (~15 mm/year, Figure 2d and Supplementary Figure 3), in agreement with previous studies (Niu et al., 2019; Yang et al., 2022). The spatial patterns of WUE (the amount of carbon gained through photosynthesis per unit of water lost through transpiration), computed as the ratio of GPP to ET, are similar to those of T and have increasing trends (Figure 2e). However, the ratio of ET to the potential ET (ET/PET) has no and decreasing (very dispersed) trends over the irrigated lands (Figure 2f). The energy demand is, therefore, laboriously met despite the increasing trends in precipitation and applied irrigated water (shown in supplementary Figure 4). The impacts of greening on T and ET are more prevalent in the Yangtze, as greening increases T (Supplementary Figure 3), while E decreases over the mixed forests (~ 3 mm/year). Though ET and WUE increase in the Yangtze, the energy demand is sufficiently met, as shown by the intensification of ET/PET. The increase in precipitation (shown in supplementary Figure 4a) is enough to meet the increasing ET demand and recharge the groundwater, consistent with Zhang et al., (2016).

3.3.Influence of greening on the seasonal dynamics of ET

Assessing the seasonality of ET as well as E and T provides a better understanding of the different behaviors observed in the two basins. ET is mainly increasing during the pre-monsoon and the monsoon (i.e., March to August) and decreases during the dry season (September to February). These trends in simulated ET by season are consistent with the trends in ET from MOD16 and GLEAM, shown in Supplementary Figure 5. Here, we present two selected periods

characterized by opposite trends, the pre-monsoon i.e., from March to May (Figure 3) and the post-monsoon or the dry season from September to November (Figure 4).

3.3.1. The pre-monsoon (March to May)

The pre-monsoon season is characterized by low ET, ET/PET, and WUE (Supplementary Figures 6, 7, and 8). The highest increases in ET (>18 mm/year; Figure 3b) in the two basins are observed in the pre-monsoon. Over the irrigated lands of the Ganges-Brahmaputra, this intensification of ET is due to irrigation through the increases in LAI. This is confirmed by the high correlation coefficients between ET and LAI and the agreements on the signs of the trends in ET and LAI shown in Supplementary Figure 9. However, though irrigation is expected to increase E, the increases in T and WUE are more significant because of greening (Figures 3d and f, Supplementary Figure 3). In the Yangtze, climate-induced greening decreases E and increases T, WUE, and ET (Figures 3b, c, d, and f, Supplementary Figures 3 and 9).

Precipitation significantly increases in the pre-monsoon period (> 50 mm/year, Figure 3e). In addition, irrigation is also performed during this season (Zhou et al., 2023). As a result, the pre-monsoon corresponding to the growing season has one of the highest rates of increases in vegetation greenness (>0.004 m^2/m^2/year, Figure 3a) and soil moisture (0.004/year, Figures 3h). The increasing ET demand driven by greening is easily met because of the trends in soil moisture. As a result, ET/PET increases (>0.02/year, Figure 3g). Though TWS decreases in the pre-monsoon as in the other seasons (45 mm/year, Figure 3i), the applied irrigated water and the increase in precipitation keep the soil sufficiently wet to meet the ET demand. Nevertheless, the limited water available (only at the soil surface) leads to enhanced control of the vegetation on ET translated by high increases in T and WUE as demonstrated by Forzieri et al., (2020) and Williams & Torn, (2015).

The increases in pre-monsoon precipitation increase LAI, soil moisture, and TWS during the growing season (Figures 3e, a, h, and i) over the Yangtze. Such a rise in water supply increases ET/PET (>0.03/year, Figure 3g). However, the increase in ET (Figure 3b) is mainly related to the increases in T (>10 mm/year, Figure 3d, also indicated by the correlation coefficients between ET and E and T and the comparisons between the signs of the trends in ET, E, and T shown in supplementary Figure 10), as greening leads to more shading of the soil surface, which decreases E (>5 mm/year, Figure 3c), thereby weakening the coupling between the atmosphere and the soil surface while increasing the plant productivity as translated by the increase in WUE.

Similar to the quantifications in Forzieri et al., (2020), these strong responses in ET to greening in the pre-monsoon are due to the high influence of LAI in the partition of surface-available energy during the growing season. In addition, the high increases in ET induced by irrigation-driven greening over the Ganges-Brahmaputra could further increase the monsoon rainfall, in particular over the mountains, because of moisture transportation (Fletcher et al., 2022).

3.3.2. The post-monsoon (dry) season (from September to November)

The post monsoon season is characterized by high ET, ET/PET, and WUE (Supplementary Figures 6, 7, and 8). ET has increasing and decreasing trends over the irrigated lands of the Ganges-Brahmaputra (Figure 4b) with ET increasing in the Himalayas foothills and the Chambal and Betwa basins. Over the croplands, the decreases in ET are linked to the decreases in E as T has no significant trends despite the greening (Figure 4c and d, Supplementary Figure 10). The post monsoon is characterized by a decreasing precipitation (25 mm/year, Figure 4e), and irrigation is not performed. Nonetheless, LAI keeps increasing (Figure 4a) likely because of the lagged influence of the monsoon while the groundwater decline influences the soil moisture (Figure 4h and i). The decline in water availability decreases ET/PET (0.025/year, Figure 4g) and affects the

crop productivity as shown by the trends in WUE. In the Chambal and Betwa basins, the soil humidity keeps increasing and is enough to maintain the ET demand, as such ET/PET rises.

In the Yangtze, the post-monsoon ET increases at a rate lower than that of the pre-monsoon (~10 mm/year, Figure 4b). Though this season corresponds to senescence, the changes in ET are attributed to both the variations of T and E, with T having the highest control as shown by the correlation coefficients in Supplementary Figure 10. Nonetheless, the WUE increases. The intensification of the post-monsoon precipitation (Figure 4e) along with the increase in snowmelt resulting from warming, enhances both soil moisture and TWS (Figure 4h and i). ET demand is, therefore, met and ET/PET increases despite the low variations of ET (0.02/year, Figure 4g). These low trends in ET are not due to the limited water availability as shown by the trends in ET/PET and WUE, rather by the energy demand, which plays an important role since ET is mostly controlled by E during that season.

In the Ganges-Brahmaputra, greening can exacerbate the decline in water availability in the post-monsoon because the limited moisture is not enough to meet the ET demand and affects the WUE. In such conditions, the increasing vegetation will pull out water from the deeper zones (Maina & Siirila-Woodburn, et al., 2022; Maina & Siirila-Woodburn, 2020; Maxwell & Condon, 2016), contributing to decreasing the groundwater storage. On the contrary, in the Yangtze, because greening is caused by climatic factors, the increases in precipitation and snowmelt are sufficient to maintain the ET demand, increase the WUE, and recharge the groundwater.

4. Conclusions

HMA's greening, caused by human activities and changes in climate, triggers different responses in ET. In the Ganges-Brahmaputra, greening induced rise of ET is dampened by groundwater depletion during the dry season. ET is mainly controlled by variations in moisture

supply rather than atmospheric demand, therefore vegetation controls ET. Because greening causes ET to significantly change during the pre-monsoon, greening could amplify the impacts of irrigation on the monsoon by intensifying land-atmosphere interactions. Nevertheless, the decrease in ET and ET/PET likely weakens the connection between the atmosphere and the land during the dry season. In addition, the limited water availability conditions impact crop productivity by affecting the WUE.

In the Yangtze, where greening is caused by climatic factors, ET, WUE, and ET/PET increase. The increases in precipitation and snowmelt are significant enough to meet the ET demand while increasing soil moisture and groundwater. Though greening is driven by climatic factors and the climate variability drives the ET patterns, these factors alone cannot explain the rise of ET, especially T and WUE (see Supplementary Figure 2 illustrating the trends in these variables when only accounting for the changes in climate). Such an increase in ET is mainly attributed to greening.

Climate and human induced greening have different effects on ET and likely the climate dynamics. Future studies can rely on climate models to study the interactions between greening and climate while incorporating the vegetation dynamics and the processes controlling water availability, such as groundwater depletion.

Acknowledgements

This research was supported by funding support from the National Aeronautics and Space Administration High Mountain Asia program (19-HMA19-0012). Computing was supported by the resources at the NASA Center for Climate Simulation.

Open Research

The NASA Land Information System (LIS) used in this study is an open-source software that can be found here: https://github.com/NASA-LIS/LISF

Datasets used in this study can be found in the following websites:

- ERA5 forcing: https://www.ecmwf.int/en/forecasts/datasets/reanalysis-datasets/era5
- IMERG Precipitation: https://gpm.nasa.gov/taxonomy/term/1372
- CHIRPS Precipitation: https://data.chc.ucsb.edu/products/CHIRPS-2.0/global_daily/netcdf/p05/
- MODIS LAI: https://lpdaac.usgs.gov/products/mcd15a2hv006/
- MODIS Snow Cover: https://nsidc.org/data/MOD10A1
- ESA CCI soil moisture: https://www.esa-soilmoisture-cci.org/data
- GRACE data: https://grace.jpl.nasa.gov/data/get-data/jpl_global_mascons/
- SWE reconstruction by Kraaijenbrink et al., (2021): https://zenodo.org/record/4715786#.YqDY0S-B1pI

References

Ambika, A. K., Wardlow, B., & Mishra, V. (2016). Remotely sensed high resolution irrigated area mapping in India for 2000 to 2015. *Scientific Data*, *3*(1), 160118. https://doi.org/10.1038/sdata.2016.118

Chen, C., Park, T., Wang, X., Piao, S., Xu, B., Chaturvedi, R. K., et al. (2019). China and India lead in greening of the world through land-use management. *Nature Sustainability*, *2*(2), 122–129. https://doi.org/10.1038/s41893-019-0220-7

Clark, A. J. (2017). Generation of Ensemble Mean Precipitation Forecasts from Convection-Allowing Ensembles. *Weather and Forecasting*, *32*(4), 1569–1583. https://doi.org/10.1175/WAF-D-16-0199.1

Cook, B. I., Puma, M. J., & Krakauer, N. Y. (2011). Irrigation induced surface cooling in the context of modern and increased greenhouse gas forcing. *Climate Dynamics*, *37*(7), 1587–1600. https://doi.org/10.1007/s00382-010-0932-x

Cortés, J., Mahecha, M. D., Reichstein, M., Myneni, R. B., Chen, C., & Brenning, A. (n.d.). Where are Global Vegetation Greening and Browning Trends Significant? *Geophysical Research Letters*, *n/a*(n/a), e2020GL091496. https://doi.org/10.1029/2020GL091496

Dickinson, R. E. (1983). Land Surface Processes and Climate—Surface Albedos and Energy Balance. In B. Saltzman (Ed.), *Advances in Geophysics* (Vol. 25, pp. 305–353). Elsevier. https://doi.org/10.1016/S0065-2687(08)60176-4

Dickinson, R. E., Shaikh, M., Bryant, R., & Graumlich, L. (1998). Interactive Canopies for a Climate Model. *Journal of Climate*, *11*(11), 2823–2836. https://doi.org/10.1175/1520-0442(1998)011<2823:ICFACM>2.0.CO;2

Douville, H., Ribes, A., Decharme, B., Alkama, R., & Sheffield, J. (2013). Anthropogenic influence on multidecadal changes in reconstructed global evapotranspiration. *Nature Climate Change*, *3*(1), 59–62. https://doi.org/10.1038/nclimate1632

Findell, K. L., Gentine, P., Lintner, B. R., & Kerr, C. (2011). Probability of afternoon precipitation in eastern United States and Mexico enhanced by high evaporation. *Nature Geoscience*, *4*(7), 434–439. https://doi.org/10.1038/ngeo1174

Fletcher, J. K., Birch, C. E., Keane, R. J., Taylor, C. M., & Folwell, S. S. (2022). The effect of Ganges river basin irrigation on pre-monsoon rainfall. *Quarterly Journal of the Royal Meteorological Society*, *148*(747), 3056–3070. https://doi.org/10.1002/qj.4218

Forzieri, G., Miralles, D. G., Ciais, P., Alkama, R., Ryu, Y., Duveiller, G., et al. (2020). Increased control of vegetation on global terrestrial energy fluxes. *Nature Climate Change*, *10*(4), 356–362. https://doi.org/10.1038/s41558-020-0717-0

Friedl, Mark, & Sulla-Menashe, Damien. (2019). MCD12Q1 MODIS/Terra+Aqua Land Cover Type Yearly L3 Global 500m SIN Grid V006 [Data set]. NASA EOSDIS Land Processes DAAC. https://doi.org/10.5067/MODIS/MCD12Q1.006

Funk, C., Peterson, P., Landsfeld, M., Pedreros, D., Verdin, J., Shukla, S., et al. (2015). The climate hazards infrared precipitation with stations—a new environmental record for monitoring extremes. *Scientific Data*, *2*(1), 150066. https://doi.org/10.1038/sdata.2015.66

Girotto, M., De Lannoy, G. J. M., Reichle, R. H., Rodell, M., Draper, C., Bhanja, S. N., & Mukherjee, A. (2017). Benefits and pitfalls of GRACE data assimilation: A case study of terrestrial water storage depletion in India. *Geophysical Research Letters*, *44*(9), 4107–4115. https://doi.org/10.1002/2017GL072994

Hersbach, H., Bell, B., Berrisford, P., Hirahara, S., Horányi, A., Muñoz-Sabater, J., et al. (2020). The ERA5 global reanalysis. *Quarterly Journal of the Royal Meteorological Society*, *146*(730), 1999–2049. https://doi.org/10.1002/qj.3803

Hock, R. (2003). Temperature index melt modelling in mountain areas. *Journal of Hydrology*, *282*(1), 104–115. https://doi.org/10.1016/S0022-1694(03)00257-9

Hu, S., & Mo, X. (2022). Diversified evapotranspiration responses to climatic change and vegetation greening in eight global great river basins. *Journal of Hydrology*, *613*, 128411. https://doi.org/10.1016/j.jhydrol.2022.128411

Huffman, G. J., Bolvin, D. T., & Nelkin, E. J. (2015). Integrated Multi-satellitE Retrievals for GPM (IMERG) technical documentation. *NASA/GSFC Code*, *612*(2015), 47.

ISRIC — World Soil Information. (n.d.). Retrieved June 21, 2022, from https://www.isric.org

Jasechko, S., Sharp, Z. D., Gibson, J. J., Birks, S. J., Yi, Y., & Fawcett, P. J. (2013). Terrestrial water fluxes dominated by transpiration. *Nature*, *496*(7445), 347–350. https://doi.org/10.1038/nature11983

Jung, M., Reichstein, M., Ciais, P., Seneviratne, S. I., Sheffield, J., Goulden, M. L., et al. (2010). Recent decline in the global land evapotranspiration trend due to limited moisture supply. *Nature*, *467*(7318), 951–954. https://doi.org/10.1038/nature09396

Kiehl, J. T., & Trenberth, K. E. (1997). Earth's Annual Global Mean Energy Budget. *Bulletin of the American Meteorological Society*, *78*(2), 197–208. https://doi.org/10.1175/1520-0477(1997)078<0197:EAGMEB>2.0.CO;2

Kraaijenbrink, P. D. A., Stigter, E. E., Yao, T., & Immerzeel, W. W. (2021). Climate change decisive for Asia's snow meltwater supply. *Nature Climate Change*, *11*(7), 591–597. https://doi.org/10.1038/s41558-021-01074-x

Kumar, S. V., Reichle, R. H., Harrison, K. W., Peters-Lidard, C. D., Yatheendradas, S., & Santanello, J. A. (2012). A comparison of methods for a priori bias correction in soil moisture data assimilation. *Water Resources Research*, *48*(3). https://doi.org/10.1029/2010WR010261

Kumar, S. V., Peters-Lidard, C. D., Mocko, D., Reichle, R., Liu, Y., Arsenault, K. R., et al. (2014). Assimilation of Remotely Sensed Soil Moisture and Snow Depth Retrievals for Drought Estimation. *Journal of Hydrometeorology*, *15*(6), 2446–2469. https://doi.org/10.1175/JHM-D-13-0132.1

Kumar, S. V., Zaitchik, B. F., Peters-Lidard, C. D., Rodell, M., Reichle, R., Li, B., et al. (2016). Assimilation of Gridded GRACE Terrestrial Water Storage Estimates in the North American Land Data Assimilation System. *Journal of Hydrometeorology*, *17*(7), 1951–1972. https://doi.org/10.1175/JHM-D-15-0157.1

Kumar, S. V., Mocko, D. M., Wang, S., Peters-Lidard, C. D., & Borak, J. (2019). Assimilation of Remotely Sensed Leaf Area Index into the Noah-MP Land Surface Model: Impacts on Water and Carbon Fluxes and States over the Continental United States. *Journal of Hydrometeorology*, *20*(7), 1359–1377. https://doi.org/10.1175/JHM-D-18-0237.1

Kumar, S. V., Jasinski, M., Mocko, D. M., Rodell, M., Borak, J., Li, B., et al. (2019). NCA-LDAS Land Analysis: Development and Performance of a Multisensor, Multivariate Land Data Assimilation System for the National Climate Assessment. *Journal of Hydrometeorology*, *20*(8), 1571–1593. https://doi.org/10.1175/JHM-D-17-0125.1

Lahmers, T. M., Kumar, S. V., Rosen, D., Dugger, A., Gochis, D. J., Santanello, J. A., et al. (2022). Assimilation of NASA's Airborne Snow Observatory Snow Measurements for Improved Hydrological Modeling: A Case Study Enabled by the Coupled LIS/WRF-Hydro System.

Water Resources Research, *58*(3), e2021WR029867. https://doi.org/10.1029/2021WR029867

Liu, X., Chen, F., Barlage, M., Zhou, G., & Niyogi, D. (2016). Noah-MP-Crop: Introducing dynamic crop growth in the Noah-MP land surface model. *Journal of Geophysical Research: Atmospheres*, *121*(23), 13,953-13,972. https://doi.org/10.1002/2016JD025597

Liu, Yongchang, Li, Z., & Chen, Y. (2021). Continuous warming shift greening towards browning in the Southeast and Northwest High Mountain Asia. *Scientific Reports*, *11*(1), 17920. https://doi.org/10.1038/s41598-021-97240-4

Liu, Yuqiong, Peters-Lidard, C. D., Kumar, S., Foster, J. L., Shaw, M., Tian, Y., & Fall, G. M. (2013). Assimilating satellite-based snow depth and snow cover products for improving snow predictions in Alaska. *Advances in Water Resources*, *54*, 208–227. https://doi.org/10.1016/j.advwatres.2013.02.005

Maina, Fadji Z., & Kumar, S. V. (2023). Diverging Trends in Rain-On-Snow Over High Mountain Asia. *Earth's Future*, *11*(3), e2022EF003009. https://doi.org/10.1029/2022EF003009

Maina, Fadji Z., Siirila-Woodburn, E. R., & Dennedy-Frank, P.-J. (2022). Assessing the impacts of hydrodynamic parameter uncertainties on simulated evapotranspiration in a mountainous watershed. *Journal of Hydrology*, *608*, 127620. https://doi.org/10.1016/j.jhydrol.2022.127620

Maina, Fadji Z., Kumar, S. V., Dollan, I. J., & Maggioni, V. (2022). Development and evaluation of ensemble consensus precipitation estimates over High Mountain Asia. *Journal of Hydrometeorology*, *1*(aop). https://doi.org/10.1175/JHM-D-21-0196.1

Maina, Fadji Zaouna, & Siirila-Woodburn, E. R. (2020). The Role of Subsurface Flow on Evapotranspiration: A Global Sensitivity Analysis. *Water Resources Research*, *56*(7), e2019WR026612. https://doi.org/10.1029/2019WR026612

Maina, Fadji Zaouna, Kumar, S. V., Albergel, C., & Mahanama, S. P. (2022). Warming, increase in precipitation, and irrigation enhance greening in High Mountain Asia. *Communications Earth & Environment*, *3*(1), 1–8. https://doi.org/10.1038/s43247-022-00374-0

Martens, B., Miralles, D. G., Lievens, H., van der Schalie, R., de Jeu, R. A. M., Fernández-Prieto, D., et al. (2017). GLEAM v3: satellite-based land evaporation and root-zone soil moisture. *Geoscientific Model Development*, *10*(5), 1903–1925. https://doi.org/10.5194/gmd-10-1903-2017

Maxwell, R. M., & Condon, L. E. (2016). Connections between groundwater flow and transpiration partitioning. *Science*, *353*(6297), 377–380. https://doi.org/10.1126/science.aaf7891

Myneni, Ranga, Knyazikhin, Yuri, & Park, Taejin. (2015). MOD15A2H MODIS/Terra Leaf Area Index/FPAR 8-Day L4 Global 500m SIN Grid V006 [Data set]. NASA EOSDIS Land Processes DAAC. https://doi.org/10.5067/MODIS/MOD15A2H.006

Nie, W., Zaitchik, B. F., Rodell, M., Kumar, S. V., Anderson, M. C., & Hain, C. (2018). Groundwater Withdrawals Under Drought: Reconciling GRACE and Land Surface Models in the United States High Plains Aquifer. *Water Resources Research*, *54*(8), 5282–5299. https://doi.org/10.1029/2017WR022178

Niu, G.-Y., & Yang, Z.-L. (2004). Effects of vegetation canopy processes on snow surface energy and mass balances. *Journal of Geophysical Research: Atmospheres*, *109*(D23). https://doi.org/10.1029/2004JD004884

Niu, G.-Y., Yang, Z.-L., Dickinson, R. E., & Gulden, L. E. (2005). A simple TOPMODEL-based runoff parameterization (SIMTOP) for use in global climate models. *Journal of Geophysical Research: Atmospheres*, *110*(D21). https://doi.org/10.1029/2005JD006111

Niu, G.-Y., Yang, Z.-L., Dickinson, R. E., Gulden, L. E., & Su, H. (2007). Development of a simple groundwater model for use in climate models and evaluation with Gravity Recovery and Climate Experiment data. *Journal of Geophysical Research: Atmospheres*, *112*(D7). https://doi.org/10.1029/2006JD007522

Niu, G.-Y., Yang, Z.-L., Mitchell, K. E., Chen, F., Ek, M. B., Barlage, M., et al. (2011). The community Noah land surface model with multiparameterization options (Noah-MP): 1. Model description and evaluation with local-scale measurements. *Journal of Geophysical Research: Atmospheres*, *116*(D12). https://doi.org/10.1029/2010JD015139

Niu, Z., He, H., Zhu, G., Ren, X., Zhang, L., Zhang, K., et al. (2019). An increasing trend in the ratio of transpiration to total terrestrial evapotranspiration in China from 1982 to 2015 caused by greening and warming. *Agricultural and Forest Meteorology*, *279*, 107701. https://doi.org/10.1016/j.agrformet.2019.107701

Oki, T., & Kanae, S. (2006). Global Hydrological Cycles and World Water Resources. *Science*, *313*(5790), 1068–1072. https://doi.org/10.1126/science.1128845

Piao, S., Yin, G., Tan, J., Cheng, L., Huang, M., Li, Y., et al. (2015). Detection and attribution of vegetation greening trend in China over the last 30 years. *Global Change Biology*, *21*(4), 1601–1609. https://doi.org/10.1111/gcb.12795

Piao, S., Wang, X., Park, T., Chen, C., Lian, X., He, Y., et al. (2020). Characteristics, drivers and feedbacks of global greening. *Nature Reviews Earth & Environment*, *1*(1), 14–27. https://doi.org/10.1038/s43017-019-0001-x

Puma, M. J., Koster, R. D., & Cook, B. I. (2013). Phenological versus meteorological controls on land-atmosphere water and carbon fluxes. *Journal of Geophysical Research: Biogeosciences*, *118*(1), 14–29. https://doi.org/10.1029/2012JG002088

Reichle, R. H., McLaughlin, D. B., & Entekhabi, D. (2002). Hydrologic Data Assimilation with the Ensemble Kalman Filter. *Monthly Weather Review*, *130*(1), 103–114. https://doi.org/10.1175/1520-0493(2002)130<0103:HDAWTE>2.0.CO;2

Reichle, R. H., Kumar, S. V., Mahanama, S. P. P., Koster, R. D., & Liu, Q. (2010). Assimilation of Satellite-Derived Skin Temperature Observations into Land Surface Models. *Journal of Hydrometeorology*, *11*(5), 1103–1122. https://doi.org/10.1175/2010JHM1262.1

Richards, L. A. (1931). Capillary conduction of liquids through porous medium. *Journal of Applied Physics*, *1*(5), 318–333. https://doi.org/10.1063/1.1745010

Running, Steve, Mu, Qiaozhen, & Zhao, Maosheng. (2017). MOD16A2 MODIS/Terra Net Evapotranspiration 8-Day L4 Global 500m SIN Grid V006 [Data set]. NASA EOSDIS Land Processes DAAC. https://doi.org/10.5067/MODIS/MOD16A2.006

Salmon, J. M., Friedl, M. A., Frolking, S., Wisser, D., & Douglas, E. M. (2015). Global rain-fed, irrigated, and paddy croplands: A new high resolution map derived from remote sensing, crop inventories and climate data. *International Journal of Applied Earth Observation and Geoinformation*, *38*, 321–334. https://doi.org/10.1016/j.jag.2015.01.014

Shen, M., Piao, S., Jeong, S.-J., Zhou, L., Zeng, Z., Ciais, P., et al. (2015). Evaporative cooling over the Tibetan Plateau induced by vegetation growth. *Proceedings of the National Academy of Sciences*, *112*(30), 9299–9304. https://doi.org/10.1073/pnas.1504418112

Sherwood, S., & Fu, Q. (2014). A Drier Future? *Science*, *343*(6172), 737–739. https://doi.org/10.1126/science.1247620

Slater, A. G., & Clark, M. P. (2006). Snow Data Assimilation via an Ensemble Kalman Filter. *Journal of Hydrometeorology*, *7*(3), 478–493. https://doi.org/10.1175/JHM505.1

Syed, T. H., Webster, P. J., & Famiglietti, J. S. (2014). Assessing variability of evapotranspiration over the Ganga river basin using water balance computations. *Water Resources Research*, *50*(3), 2551–2565. https://doi.org/10.1002/2013WR013518

Viviroli, D., Dürr, H. H., Messerli, B., Meybeck, M., & Weingartner, R. (2007). Mountains of the world, water towers for humanity: Typology, mapping, and global significance. *Water Resources Research*, *43*(7). https://doi.org/10.1029/2006WR005653

Webster, P. J., Jian, J., Hopson, T. M., Hoyos, C. D., Agudelo, P. A., Chang, H.-R., et al. (2010). Extended-Range Probabilistic Forecasts of Ganges and Brahmaputra Floods in Bangladesh. *Bulletin of the American Meteorological Society*, *91*(11), 1493–1514. https://doi.org/10.1175/2010BAMS2911.1

Williams, I. N., & Torn, M. S. (2015). Vegetation controls on surface heat flux partitioning, and land-atmosphere coupling. *Geophysical Research Letters*, *42*(21), 9416–9424. https://doi.org/10.1002/2015GL066305

Xue, Y., Houser, P. R., Maggioni, V., Mei, Y., Kumar, S. V., & Yoon, Y. (2019). Assimilation of Satellite-Based Snow Cover and Freeze/Thaw Observations Over High Mountain Asia. *Frontiers in Earth Science*, *7*. https://doi.org/10.3389/feart.2019.00115

Xue, Y., Houser, P. R., Maggioni, V., Mei, Y., Kumar, S. V., & Yoon, Y. (2022). Evaluation of High Mountain Asia-Land Data Assimilation System (Version 1) From 2003 to 2016: 2. The Impact of Assimilating Satellite-Based Snow Cover and Freeze/Thaw Observations Into a Land Surface Model. *Journal of Geophysical Research: Atmospheres*, *127*(7), e2021JD035992. https://doi.org/10.1029/2021JD035992

Yamazaki, D., Ikeshima, D., Tawatari, R., Yamaguchi, T., O'Loughlin, F., Neal, J. C., et al. (2017). A high-accuracy map of global terrain elevations. *Geophysical Research Letters*, *44*(11), 5844–5853. https://doi.org/10.1002/2017GL072874

Yang, Z., Bai, P., & Li, Y. (2022). Quantifying the effect of vegetation greening on evapotranspiration and its components on the Loess Plateau. *Journal of Hydrology*, *613*, 128446. https://doi.org/10.1016/j.jhydrol.2022.128446

Zaitchik, B. F., Rodell, M., & Reichle, R. H. (2008). Assimilation of GRACE Terrestrial Water Storage Data into a Land Surface Model: Results for the Mississippi River Basin. *Journal of Hydrometeorology*, *9*(3), 535–548. https://doi.org/10.1175/2007JHM951.1

Zeng, Z., Piao, S., Lin, X., Yin, G., Peng, S., Ciais, P., & Myneni, R. B. (2012). Global evapotranspiration over the past three decades: estimation based on the water balance equation combined with empirical models. *Environmental Research Letters*, *7*(1), 014026. https://doi.org/10.1088/1748-9326/7/1/014026

Zeng, Z., Wang, T., Zhou, F., Ciais, P., Mao, J., Shi, X., & Piao, S. (2014). A worldwide analysis of spatiotemporal changes in water balance-based evapotranspiration from 1982 to 2009. *Journal of Geophysical Research: Atmospheres*, *119*(3), 1186–1202. https://doi.org/10.1002/2013JD020941

Zeng, Z., Zhu, Z., Lian, X., Li, L. Z. X., Chen, A., He, X., & Piao, S. (2016). Responses of land evapotranspiration to Earth's greening in CMIP5 Earth System Models. *Environmental Research Letters*, *11*(10), 104006. https://doi.org/10.1088/1748-9326/11/10/104006

Zeng, Z., Piao, S., Li, L. Z. X., Zhou, L., Ciais, P., Wang, T., et al. (2017). Climate mitigation from vegetation biophysical feedbacks during the past three decades. *Nature Climate Change*, *7*(6), 432–436. https://doi.org/10.1038/nclimate3299

Zeng, Z., Piao, S., Li, L. Z. X., Wang, T., Ciais, P., Lian, X., et al. (2018). Impact of Earth Greening on the Terrestrial Water Cycle. *Journal of Climate*, *31*(7), 2633–2650. https://doi.org/10.1175/JCLI-D-17-0236.1

Zeng, Z., Peng, L., & Piao, S. (2018). Response of terrestrial evapotranspiration to Earth's greening. *Current Opinion in Environmental Sustainability*, *33*, 9–25. https://doi.org/10.1016/j.cosust.2018.03.001

Zhang, K., Kimball, J. S., Nemani, R. R., Running, S. W., Hong, Y., Gourley, J. J., & Yu, Z. (2015). Vegetation Greening and Climate Change Promote Multidecadal Rises of Global Land Evapotranspiration. *Scientific Reports*, *5*(1), 15956. https://doi.org/10.1038/srep15956

Zhang, Y., Peña-Arancibia, J. L., McVicar, T. R., Chiew, F. H. S., Vaze, J., Liu, C., et al. (2016). Multi-decadal trends in global terrestrial evapotranspiration and its components. *Scientific Reports*, *6*(1), 19124. https://doi.org/10.1038/srep19124

Zhu, Z., Piao, S., Myneni, R. B., Huang, M., Zeng, Z., Canadell, J. G., et al. (2016). Greening of the Earth and its drivers. *Nature Climate Change*, *6*(8), 791–795. https://doi.org/10.1038/nclimate3004

Figure Caption

Figure 1: High Mountain Asia (a) land cover derived from MODIS (Friedl, Mark & Sulla-Menashe, Damien, 2019) and (b) the percent of irrigated areas (Salmon et al., 2015).

Figure 2: Spatial distributions of the statistically significant annual trends in (a) LAI, (b) ET, (c) E, (d) T, (e) WUE, and (f) ET/PET; (g) represents the trends detection of ET compared to MOD16 and GLEAM.

Figure 3: Spatial distributions of the statistically significant pre-monsoon trends in (a) LAI, (b) ET, (c) E, (d) T, (e) P, (f) WUE, (g) ET/PET, (h) soil moisture, and (i) TWS.

Figure 4: Spatial distributions of the statistically significant post-monsoon trends in (a) LAI, (b) ET, (c) E, (d) T, (e) P, (f) WUE, (g) ET/PET, (h) soil moisture, and (i) TWS.

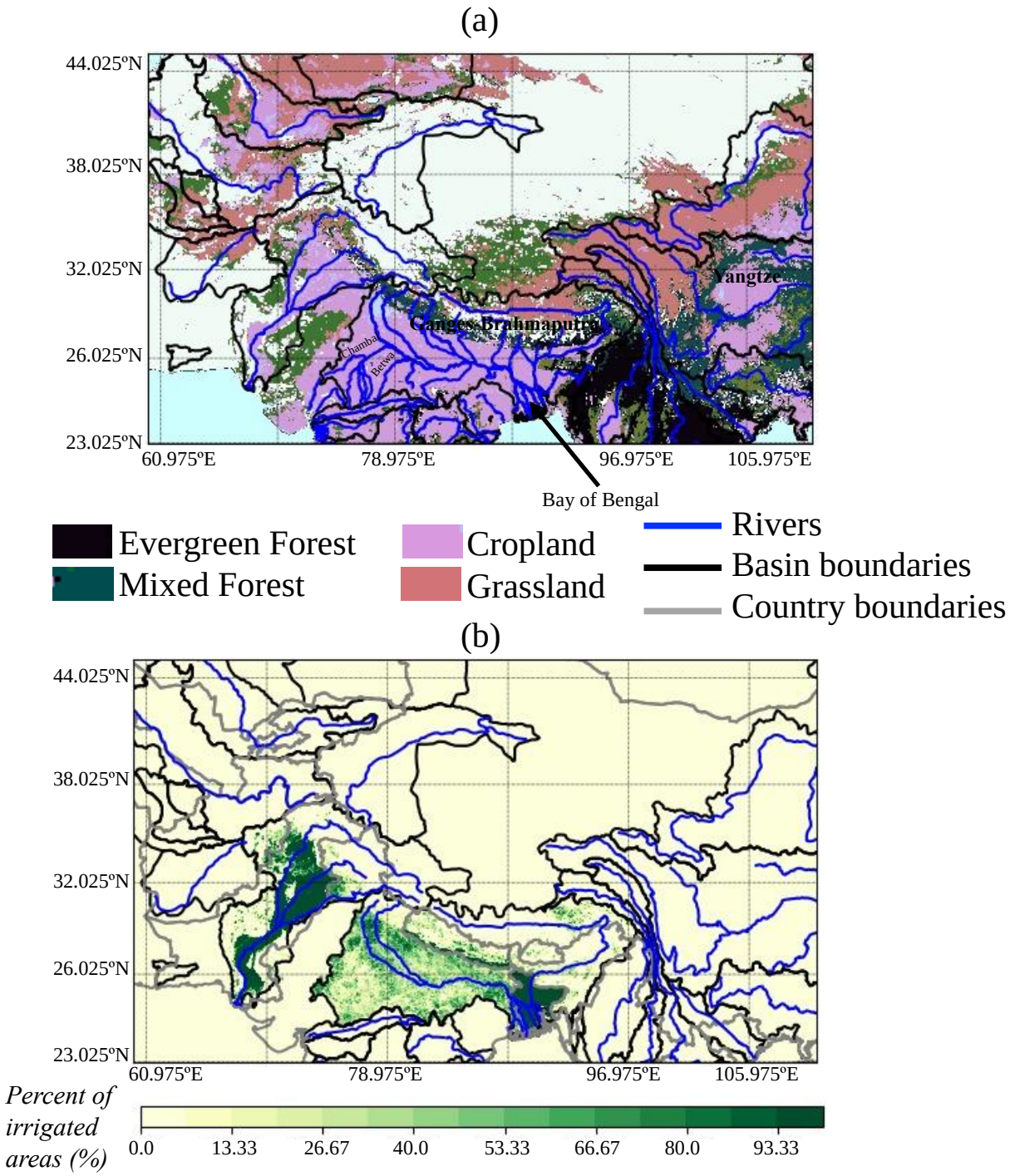

586

587 Figure 1: High Mountain Asia (a) land cover derived from MODIS (Friedl, Mark & Sulla-

588 Menashe, Damien, 2019) and (b) the percent of irrigated areas (Salmon et al., 2015).

589

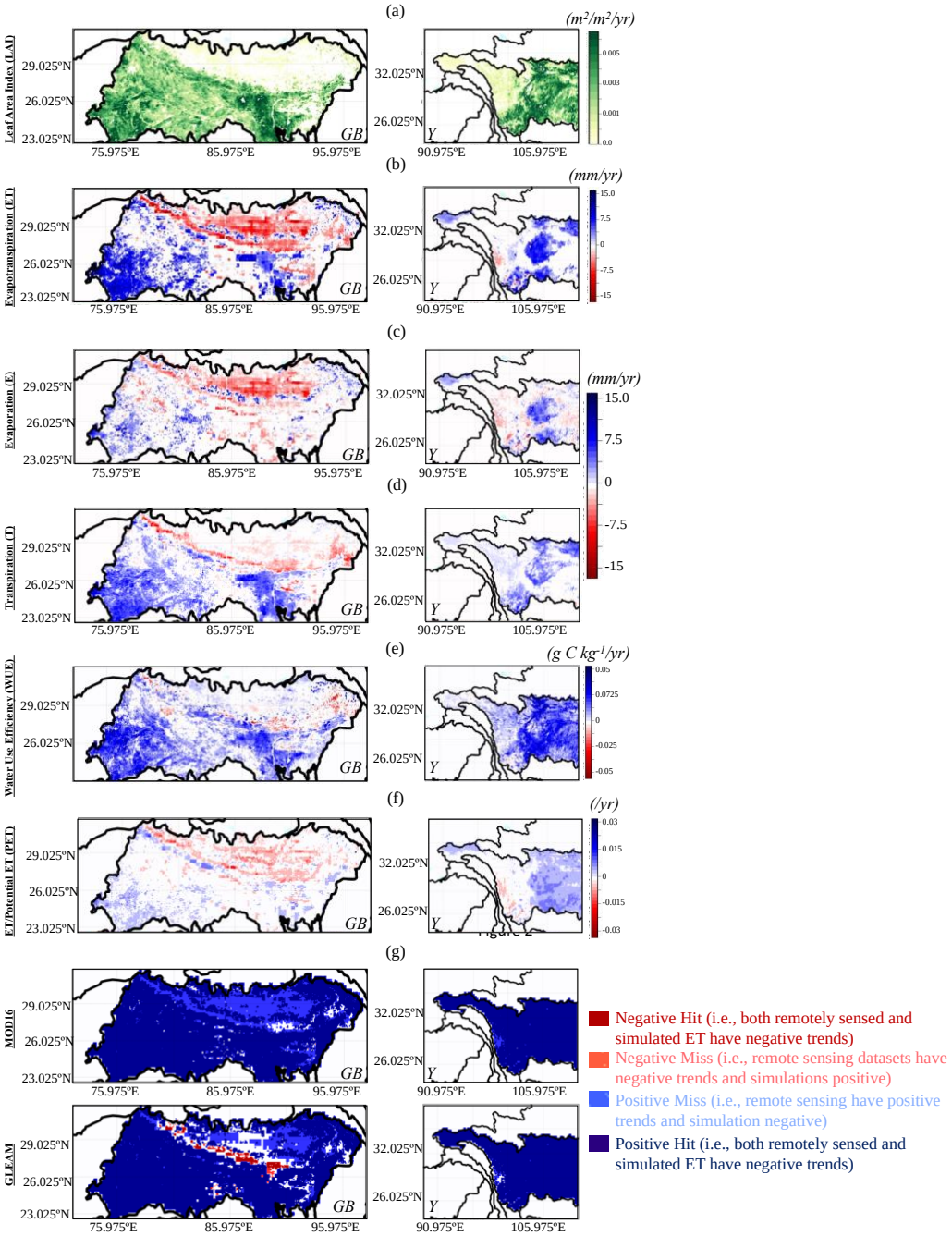

590

591 Figure 2: Spatial distributions of the statistically significant annual trends in (a) LAI, (b) ET, (c)

592 E, (d) T, (e) WUE, and (f) ET/PET; (g) represents the trends detection of ET compared to MOD16

593 and GLEAM.

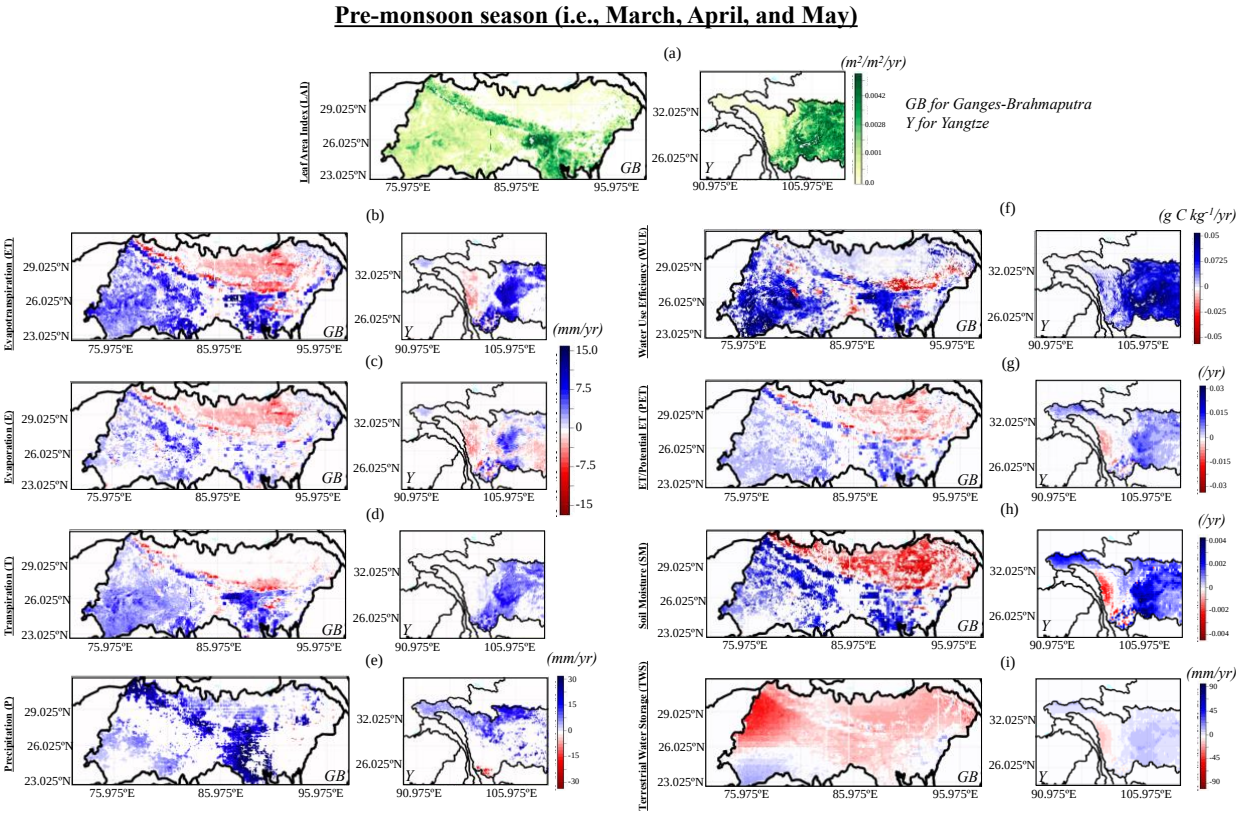

Figure 3: Spatial distributions of the statistically significant pre-monsoon trends in (a) LAI, (b) ET, (c) E, (d) T, (e) P, (f) WUE, (g) ET/PET, (h) soil moisture, and (i) TWS.

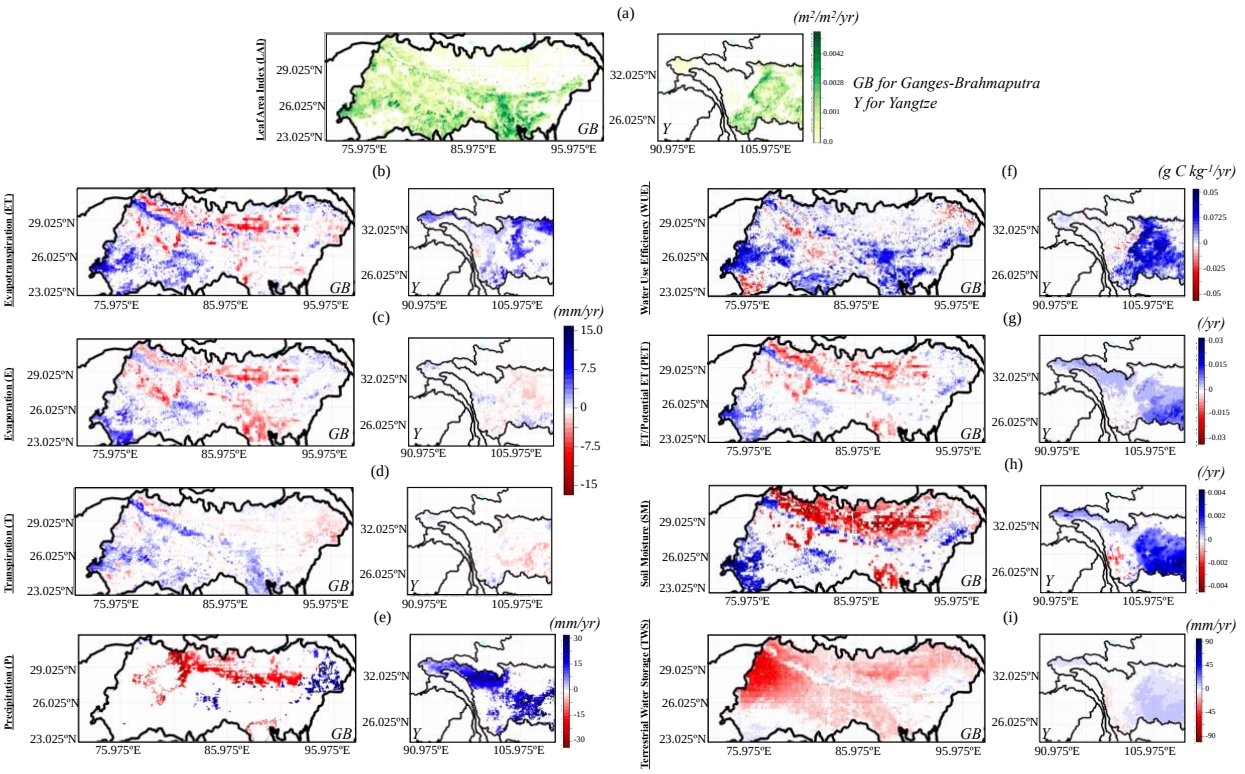

Figure 4: Spatial distributions of the statistically significant post-monsoon trends in (a) LAI, (b) ET, (c) E, (d) T, (e) P, (f) WUE, (g) ET/PET, (h) soil moisture, and (i) TWS.

Supporting Information

Variables	Type	Standard Deviation	Temporal Correlation	Perturbation cross-correlations
Forcing				
Precipitation	M	0.2	24h	1.0 -0.5 -0.8
Shortwave Radiation	M	30	24h	-0.5 1.0 0.5
Longwave Radiation	A	0.50	24h	-0.8 0.5 1.0
Assimilation of Soil Moisture				
ESA CCI Soil Moisture	A	0.02	12h	
Modeled Soil Moisture Layer 1	A	0.1	3h	1.0 0.6 0.4 0.2
Modeled Soil Moisture Layer 2	A	0.1	3h	0.6 1.0 0.6 0.4
Modeled Soil Moisture Layer 3	A	0.1	3h	0.4 0.6 1.0 0.6
Modeled Soil Moisture Layer 4	A	0.1	3h	0.2 0.4 0.6 1.0
Assimilation of LAI				
MODIS LAI	A	0.01	1 h	
Modeled LAI	A	0.01	1h	
Assimilation of SWE				
SWE Reconstruction	M	0.05	3h	
Modeled Snow Depth	M	0.01	3h	1.0 0.9
Modeled SWE	M	0.01	3h	0.9 1.0
Assimilation of GRACE				
GRACE TWS	A	5.0	24h	
Modeled Soil Moisture Layer 1	A	0.005	3h	1.0 0.6 0.4 0.2 0.0 0.0
Modeled Soil Moisture Layer 2	A	0.005	3h	0.6 1.0 0.6 0.4 0.0 0.0
Modeled Soil Moisture Layer 3	A	0.005	3h	0.4 0.6 1.0 0.6. 0.0 0.0
Modeled Soil Moisture Layer 4	A	0.005	3h	0.2 0.4 0.6 1.0 0.0 0.0
Modeled Groundwater Storage	A	0.1	3h	0.0 0.0 0.0 0.0 0.0 1.0 0.0
Modeled SWE	M	0.001	30min	0.0 0.0 0.0 0.0 0.0 0.0 1.0

Supplementary Table 1: Applied perturbations for the multivariate data assimilation

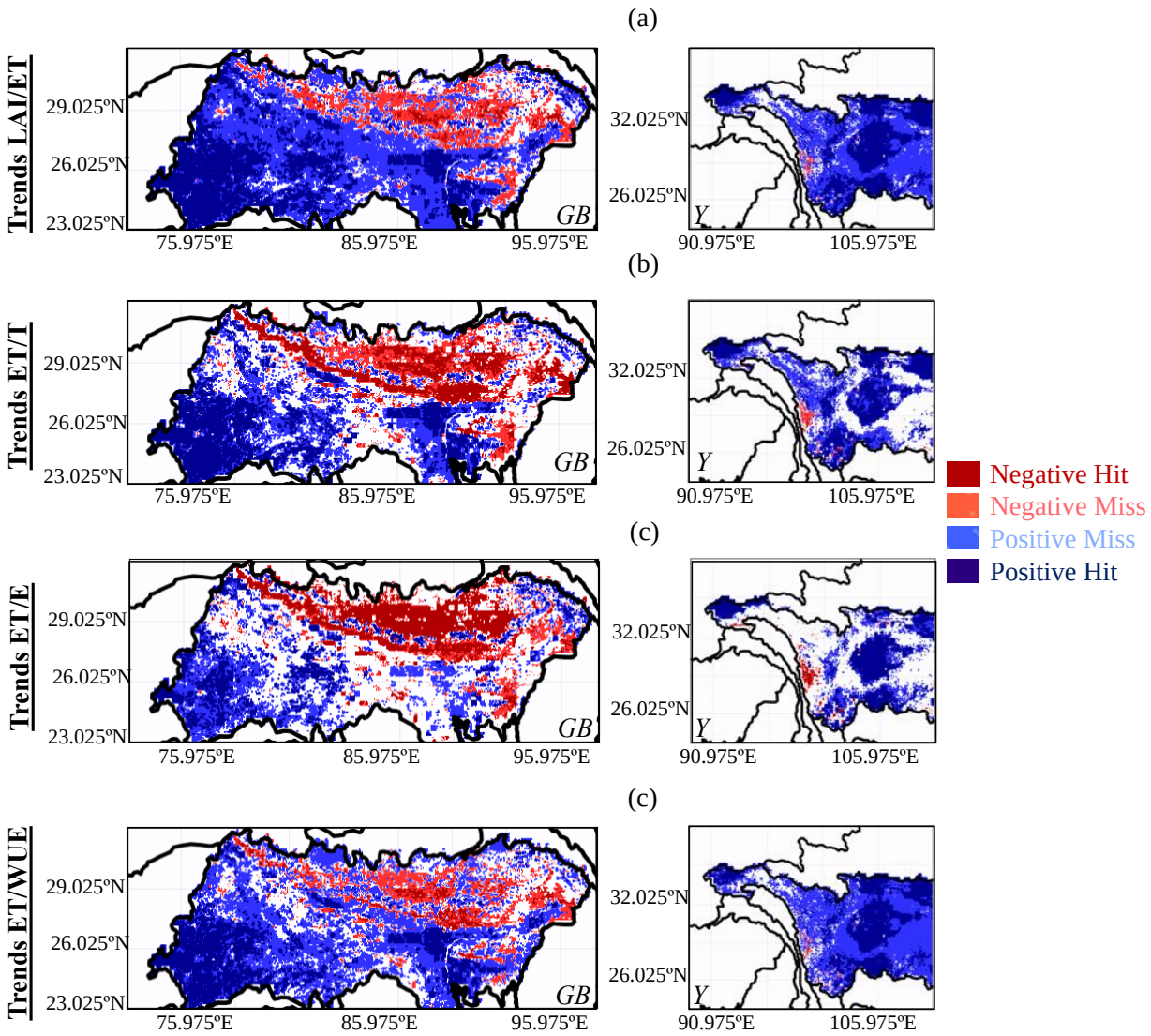

Supplementary Figure 1: The trends detection of gross primary productivity (GPP) compared to MODIS. "Negative Hit" corresponds to locations where both remotely sensed and simulated GPP have negative trends, in "Negative Miss" remote sensing have negative trends and simulations positive, in "Positive Hit" both remotely sensed and simulated GPP have negative trends, and in "Positive Miss" remote sensing have positive trends and simulation negative.

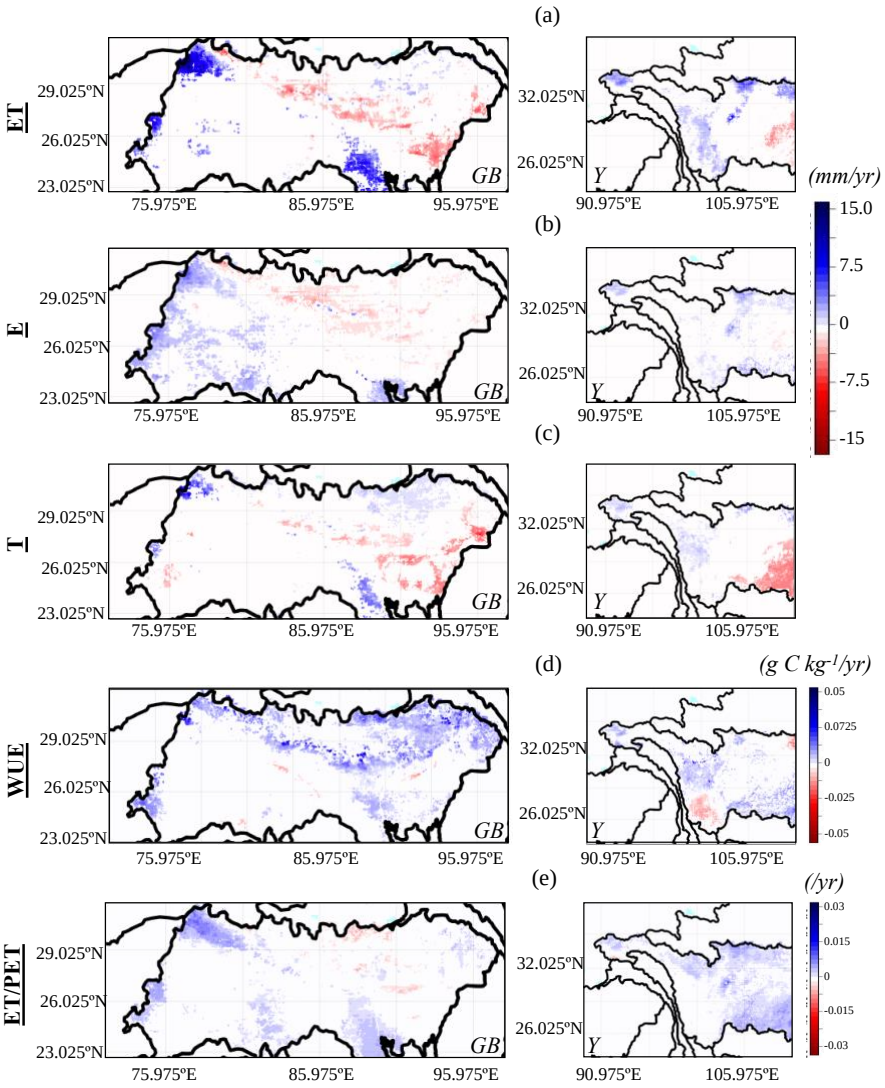

Supplementary Figure 2: Spatial distributions of the open-loop trends in (a) Evapotranspiration (ET), (b) Evaporation (E), (c) Transpiration (T), (d) the water use efficiency (WUE) defined as the ratio of the gross primary production (GPP) to the evapotranspiration (ET), and (f) the ratio of evapotranspiration (ET) to the potential evapotranspiration (PET) i.e., ET/PET over the Ganges-Brahmaputra (GB) and the Yangtze (Y). The open-loop simulation was performed without accounting for the impacts of greening and groundwater depletion. The trends were computed from 2003 to 2020 using the Mann-Kendall test with a confidence level of 95%, non-significant trends were set to 0.

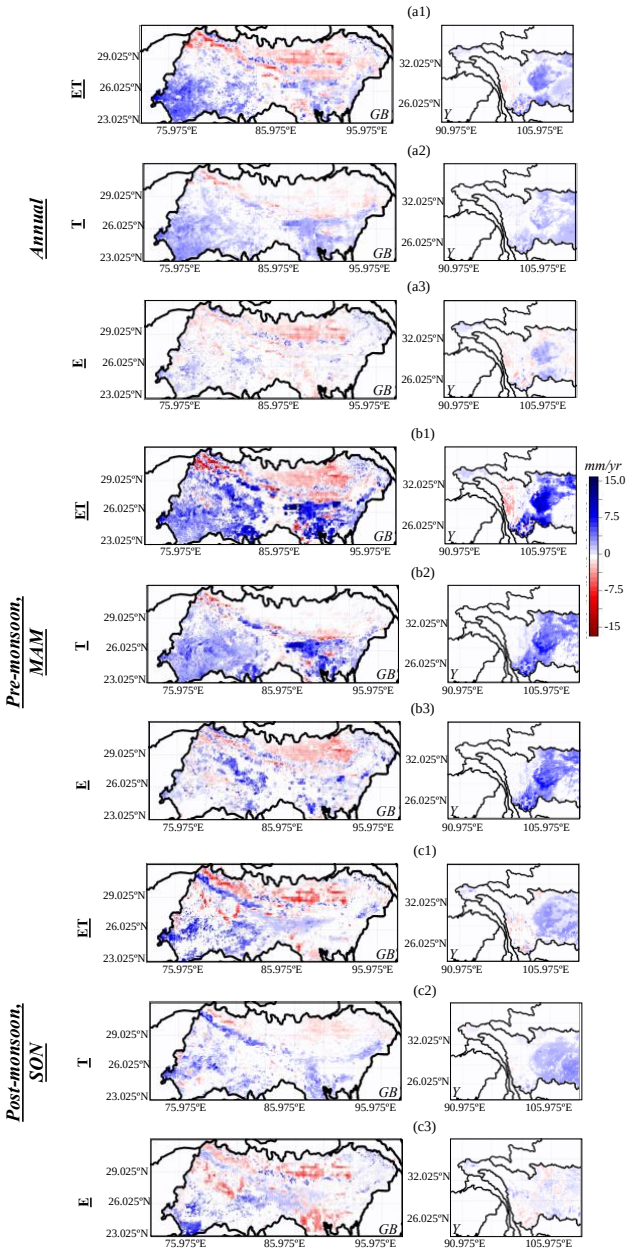

623

624 Supplementary Figure 3: Differences in the trends in ET (with subscript 1), T (with subscript 2),
625 and E (with subscript 3) obtained with the open loop (i.e., simulation without the impacts of
626 greening and groundwater depletion) and the multivariate assimilation (i.e., simulation accounting
627 for the impacts of greening and groundwater depletion). Blue indicates areas where the
628 multivariate assimilation has higher values than the open loop and red the opposite. This figure
629 depicts the intensification of ET and its components triggered by greening.

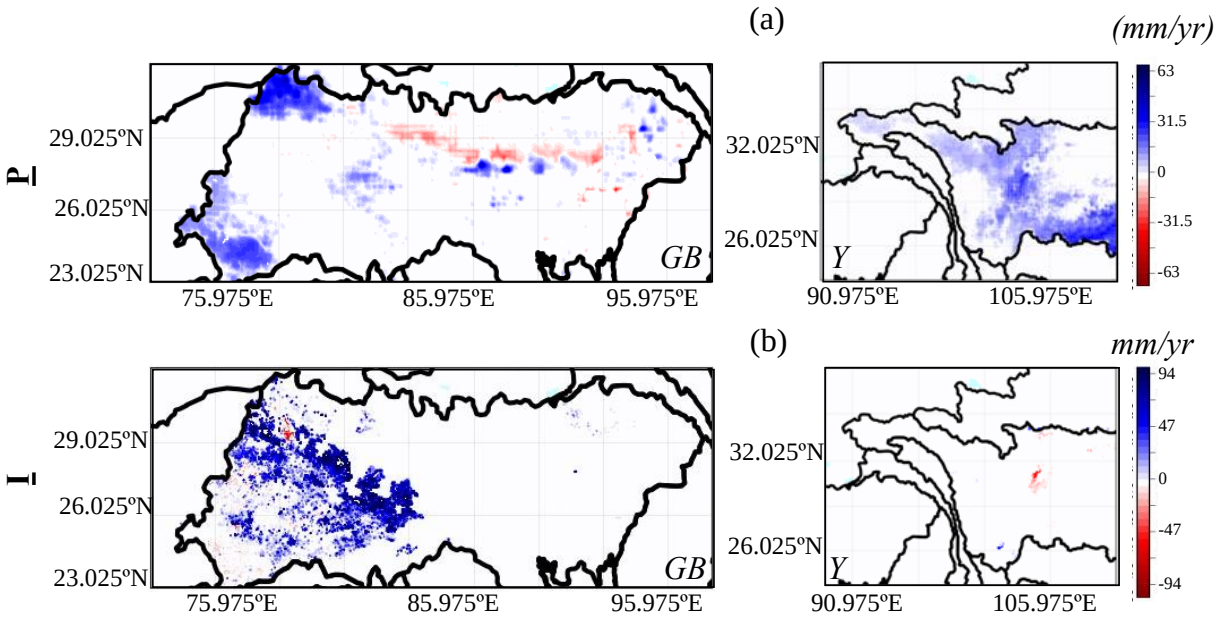

Supplementary Figure 4: Spatial distributions of trends in (a) precipitation (P) and (b) applied irrigated water over the Ganges-Brahmaputra (GB) and the Yangtze (Y). The trends were computed from 2003 to 2020 using the Mann-Kendall test with a confidence level of 95%, non-significant trends were set to 0.

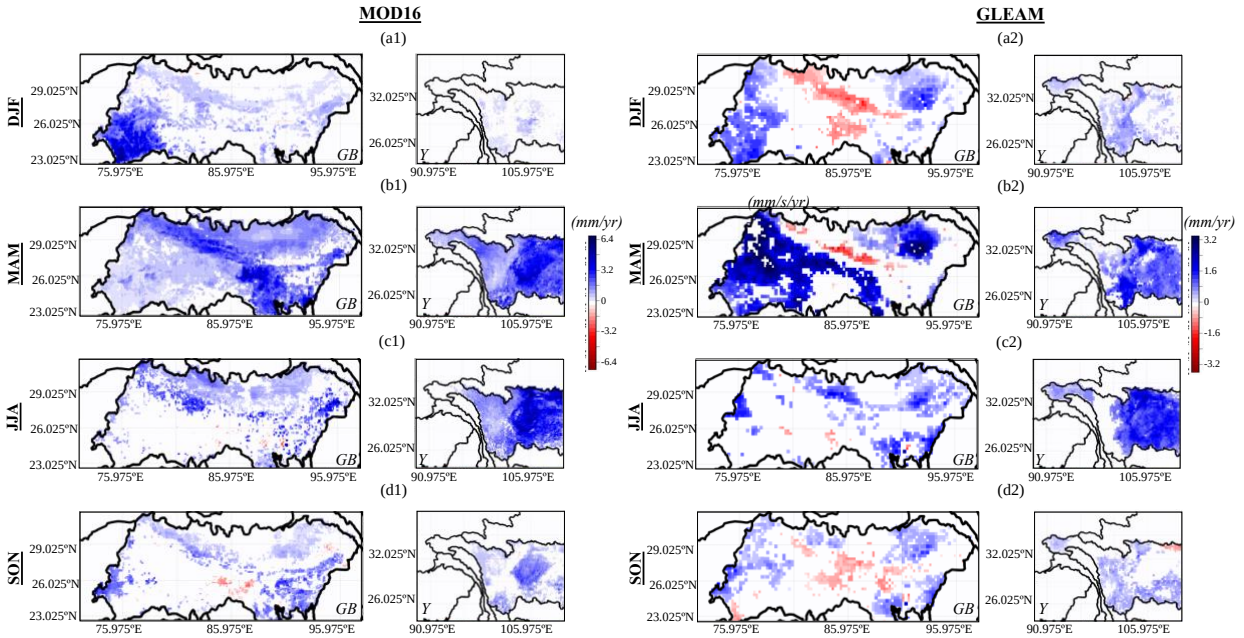

Supplementary Figure 5: Spatial distributions of trends in Evapotranspiration (ET) from the Moderate Resolution Imaging Spectroradiometer (MODIS, MOD16) and the Global Land Evaporation Amsterdam Model (GLEAM) over the Ganges-Brahmaputra (GB) and the Yangtze (Y). The trends are computed for the four seasons (December-January-February DJF, March-April-May MAM, June-July-August JJA, and September-October-November, SON). The trends were computed from 2003 to 2020 using the Mann-Kendall test with a confidence level of 95%, non-significant trends were set to 0.

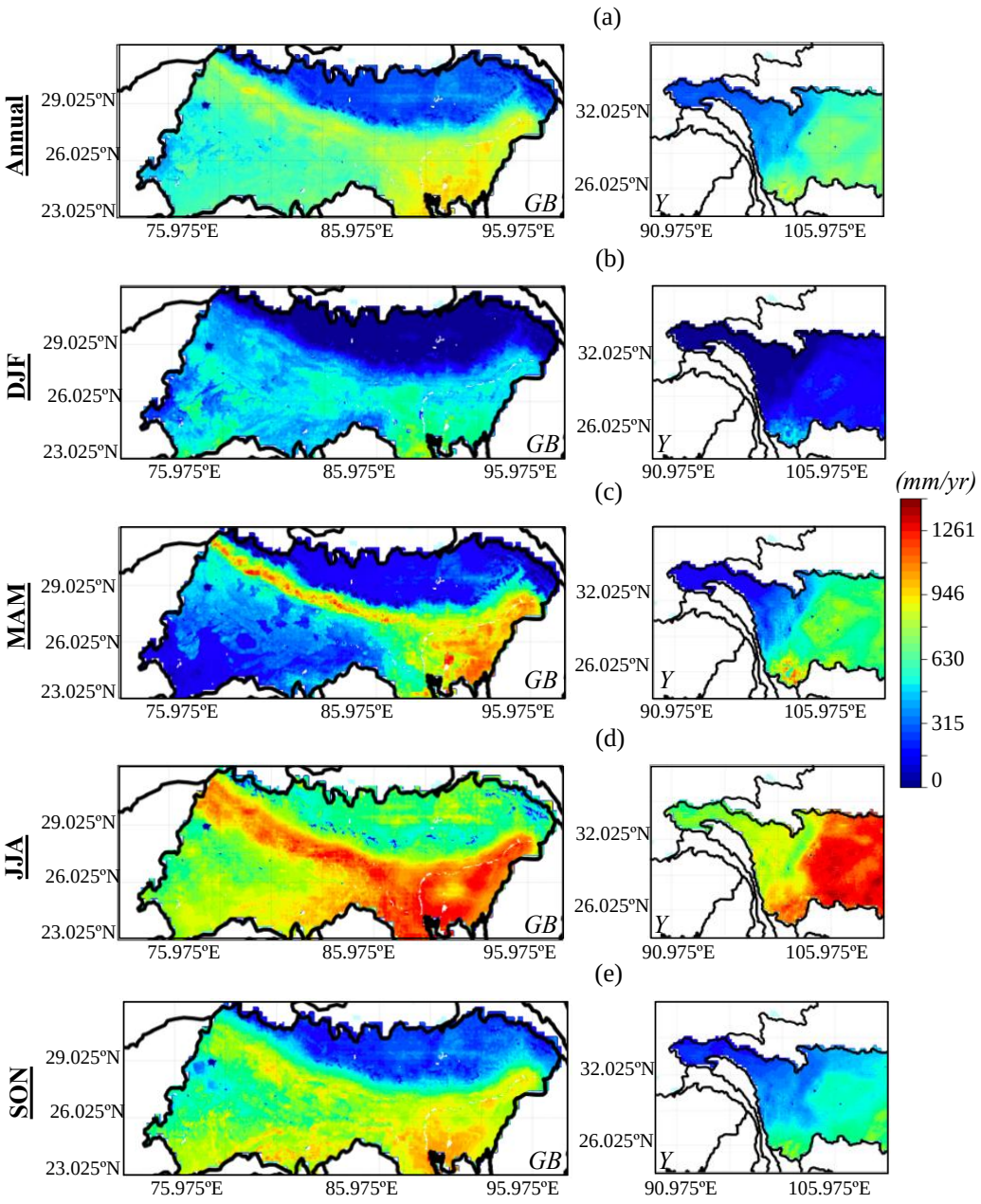

Supplementary Figure 6: Spatial distributions of the (a) annual average Evapotranspiration (ET) and the annual average of the four seasons ((b) December-January-February DJF, (c) March-April-May MAM, (d) June-July-August JJA, and (e) September-October-November, SON) over the Ganges-Brahmaputra (GB) and the Yangtze (Y).

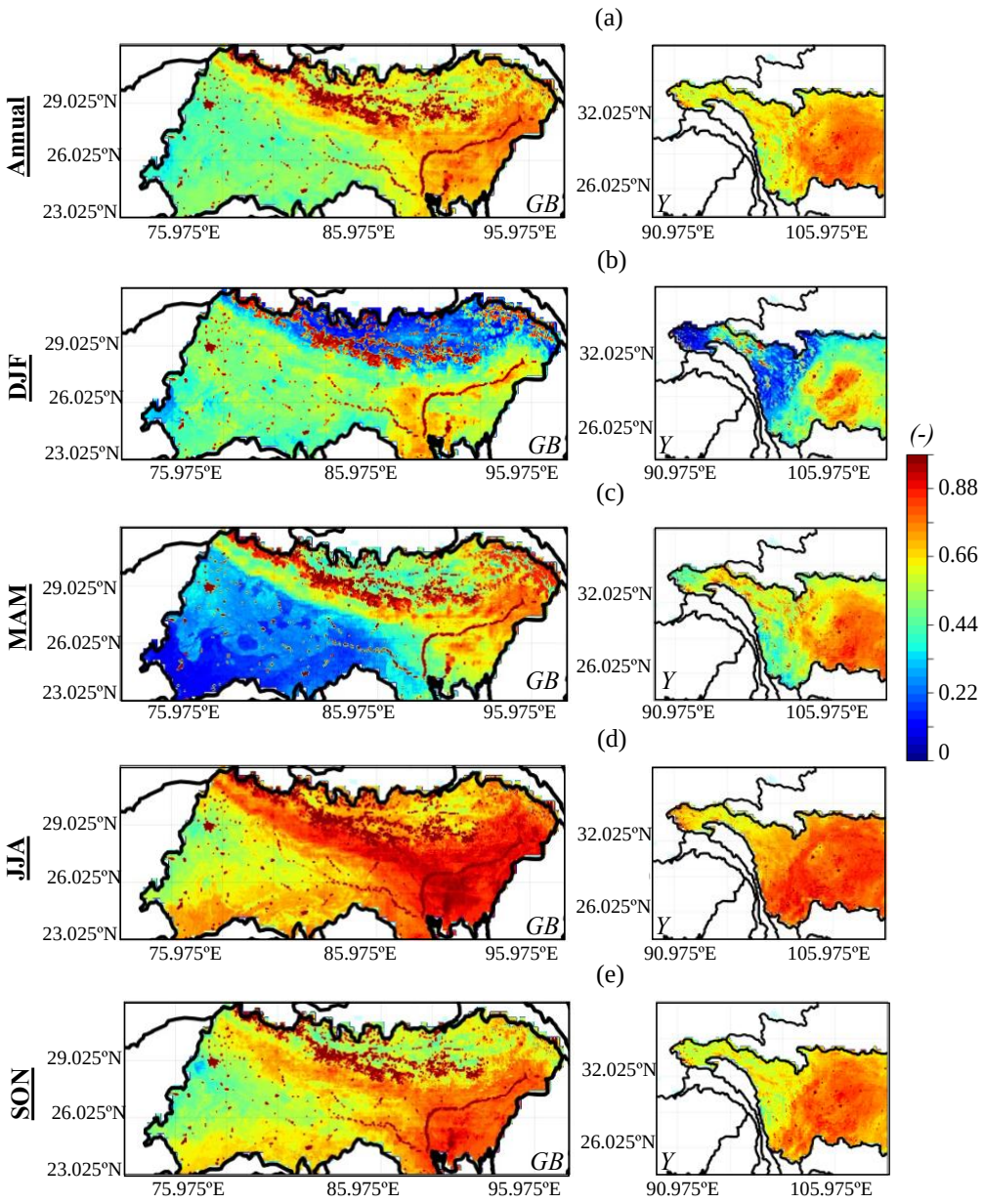

Supplementary Figure 7: Spatial distributions of the (a) annual average of the ratio of evapotranspiration (ET) to the potential evapotranspiration (PET) i.e., ET/PET and the annual average of the four seasons ((b) December-January-February DJF, (c) March-April-May MAM, (d) June-July-August JJA, and (e) September-October-November, SON) over the Ganges-Brahmaputra (GB) and the Yangtze (Y).

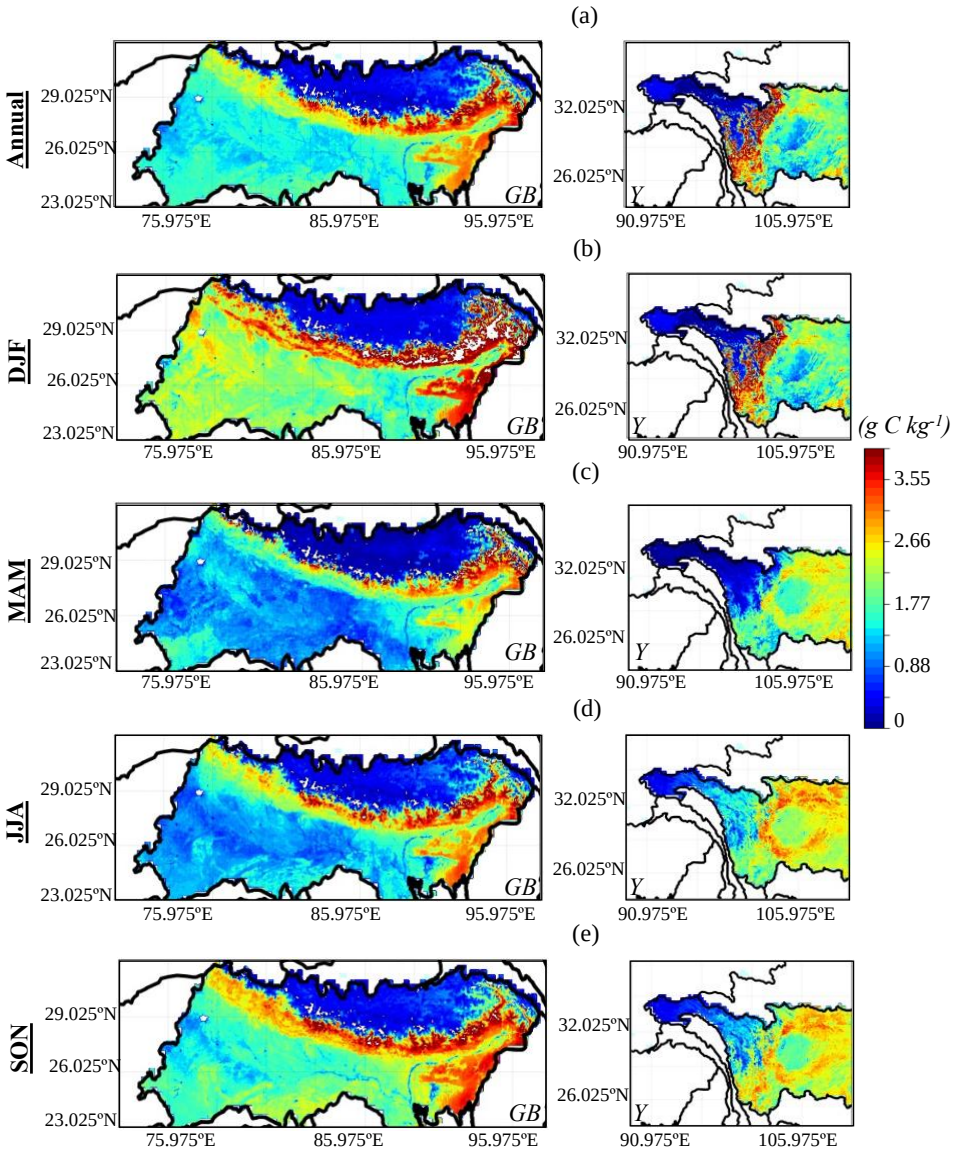

Supplementary Figure 8: Spatial distributions of the (a) annual average of the water use efficiency (WUE) defined as the ratio of the gross primary production (GPP) to the evapotranspiration (ET) and the annual average of the four seasons ((b) December-January-February DJF, (c) March-April-May MAM, (d) June-July-August JJA, and (e) September-October-November, SON) over the Ganges-Brahmaputra (GB) and the Yangtze (Y).

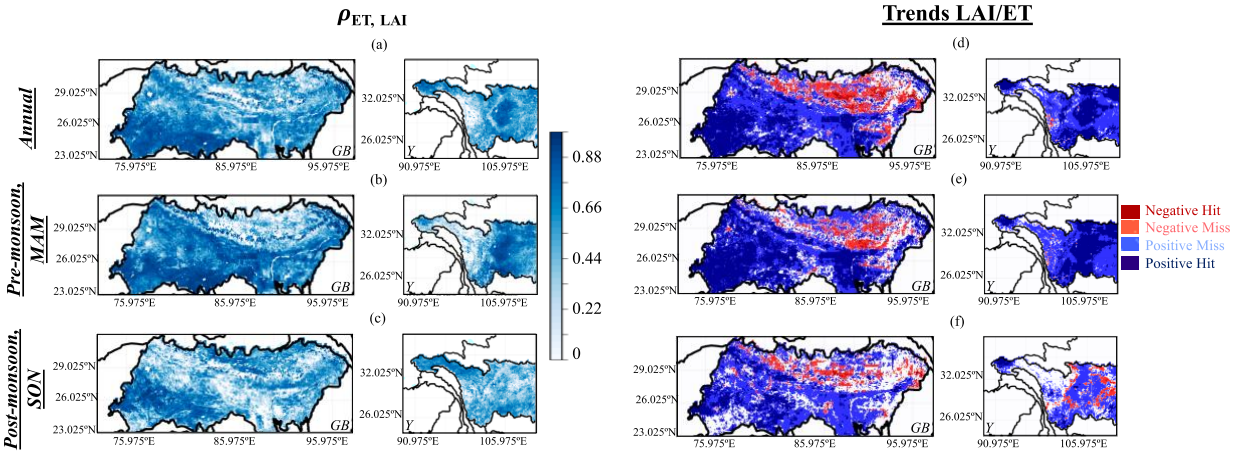

Supplementary Figure 9: Pearson's correlation coefficients between ET and LAI (a) on the annual scale, and during the (b) pre-monsoon and (b) post-monsoon. Comparisons between the trends in ET and LAI (d) on the annual scale, and during the (e) pre-monsoon and (f) post-monsoon. Negative Hit means that both ET and LAI have negative trends, Negative Miss is when ET has a negative trend and LAI a positive trend, Positive Miss is when ET has a positive trend and LAI a negative trend, and Positive Hit is when both ET and LAI have positive trends.

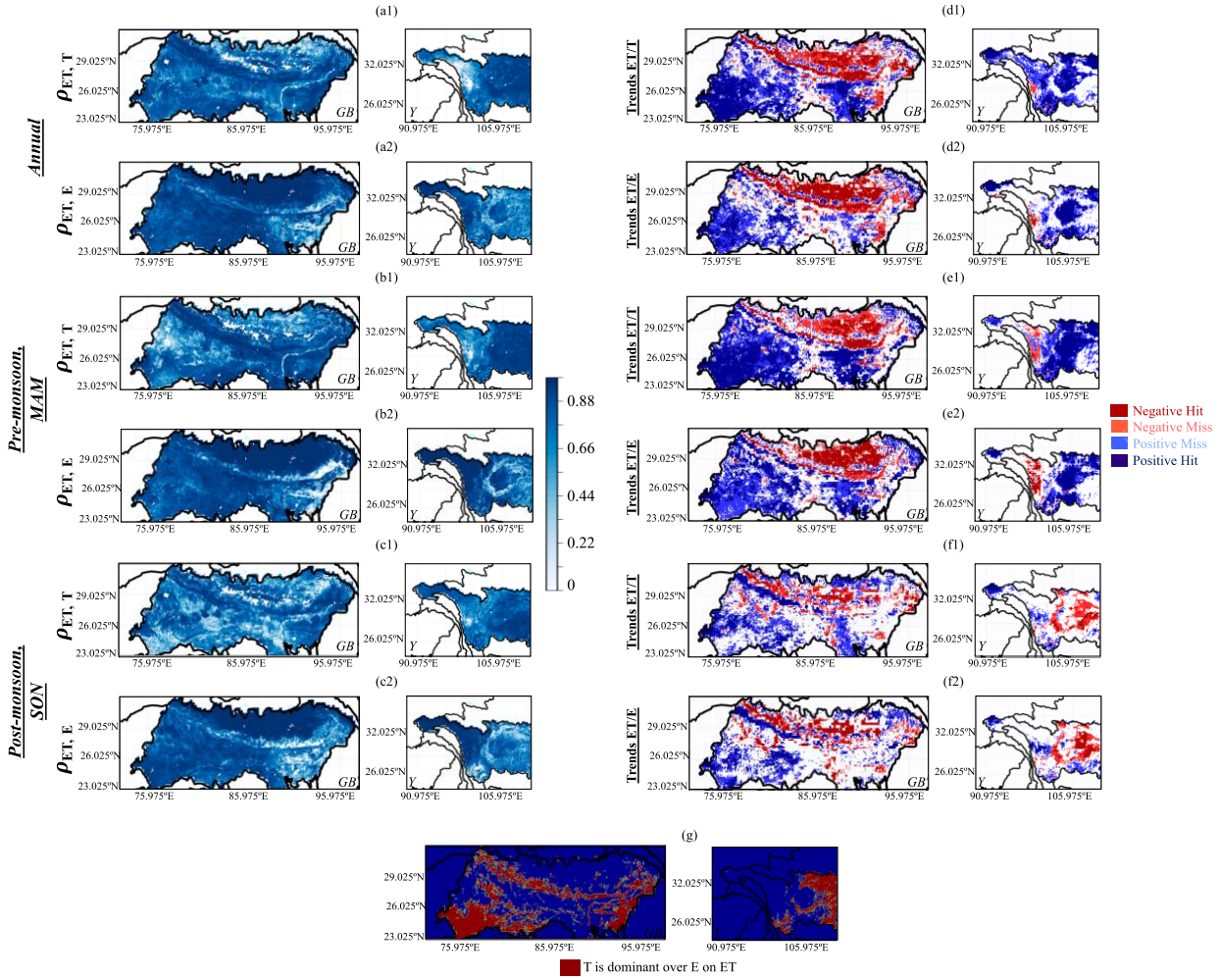

Supplementary Figure 10: Pearson's correlation coefficients between ET and T (with subscript 1) and E (with subscript 2) (a) on the annual scale, and during the (b) pre-monsoon and (b) post-monsoon. Comparisons between the trends in ET and T (with subscript 1) and E (with subscript 2) (d) on the annual scale, and during the (e) pre-monsoon and (f) post-monsoon. Negative Hit means that both ET and T/E have negative trends, Negative Miss is when ET has a negative trend and T/E a positive trend, Positive Miss is when ET has a positive trend and T/E a negative trend, and Positive Hit is when both ET and T/E have positive trends. (g) areas where the transpiration T is the dominant driver to ET (i.e., ratio of T/ET is greater than 0.5) on the annual scale.